

Limited Intermixing of Synaptic Vesicle Components upon Vesicle Recycling

Felipe Opazo¹, Annedore Punge², Johanna Bückers², Peer Hoopmann¹, Lars Kastrop², Stefan W. Hell² and Silvio O. Rizzoli^{1,*}

¹European Neuroscience Institute Göttingen (ENI-G), DFG Research Center for Molecular Physiology of the Brain (CMPB)/Excellence Cluster 171, Grisebachstr. 5, 37077 Göttingen, Germany

²Department of Nanobiophotonics, Max Planck Institute for Biophysical Chemistry, Am Fassberg 11, 37077 Göttingen, Germany

*Corresponding author: Silvio O Rizzoli, S.Rizzoli@eni-g.de

Synaptic vesicles recycle repeatedly in order to maintain synaptic transmission. We have previously proposed that upon exocytosis the vesicle components persist as clusters, which would be endocytosed as whole units. It has also been proposed that the vesicle components diffuse into the plasma membrane and are then randomly gathered into new vesicles. We found here that while strong stimulation (releasing the entire recycling pool) causes the diffusion of the vesicle marker synaptotagmin out of synaptic boutons, moderate stimulation (releasing ~19% of all vesicles) is followed by no measurable diffusion. In agreement with this observation, synaptotagmin molecules labeled with different fluorescently tagged antibodies did not appear to mix upon vesicle recycling, when investigated by subdiffraction resolution stimulated emission depletion (STED) microscopy. Finally, as protein diffusion from vesicles has been mainly observed using molecules tagged with pH-sensitive green fluorescent protein (pHluorin), we have also investigated the membrane patterning of several native and pHluorin-tagged proteins. While the native proteins had a clustered distribution, the GFP-tagged ones were diffused in the plasma membrane. We conclude that synaptic vesicle components intermix little, at least under moderate stimulation, possibly because of the formation of clusters in the plasma membrane. We suggest that several pHluorin-tagged vesicle proteins are less well integrated in clusters.

Key words: high resolution, hippocampal, pHluorin, STED, synaptic vesicle

Received 12 October 2009, revised and accepted for publication 3 March 2010, uncorrected manuscript published online 9 March 2010, published online 5 April 2010

Synaptic vesicle recycling is a fundamental process in neuronal communication, with its first step being neurotransmitter release through vesicle fusion with the plasma membrane (exocytosis). Two main models of vesicle

fusion have been proposed: kiss-and-run, in which the vesicle fuses transiently with the plasma membrane, and is retrieved simply by closure of the fusion pore, and full fusion, in which the vesicle collapses into the plasma membrane. In this second alternative, the vesicle components are gathered by the recycling machinery, and a new vesicle is invaginated (endocytosis), typically by clathrin and its associated factors. The resulting vesicle may undergo a subsequent sorting step by fusing with an early (sorting) endosome or may form a mature vesicle by losing the clathrin coat (1,2).

While kiss-and-run assumes that the identity of the vesicle is maintained during recycling, this issue is much more difficult to predict for full fusion. Vesicle material may diffuse into the plasma membrane, to be later randomly gathered by the endocytosis machinery, or may remain as clusters, which would then serve as targets for clathrin and associated factors. As following synaptic vesicle material fused onto the plasma membrane requires its specific labeling, most experiments targeting this issue have been performed using pHluorins (3), which are pH-sensitive green fluorescent protein (GFP) variants linked to intravesicular regions of synaptic vesicle proteins. The pHluorins are quenched by the acidity in the organelles (at a pH of approximately 5–6). Upon exocytosis, the GFP moieties find themselves in a neutral pH environment, and their fluorescence increases substantially (4).

Two main lines of evidence suggest that pHluorin-tagged molecules may not remain grouped as units (as fused vesicles) upon exocytosis. First, stimulation causes a strong diffusion of pHluorin-tagged proteins out of synapses and into the axonal space, as demonstrated using synaptobrevin-GFP (5), synaptobrevin-pHluorin (6,7) and synaptophysin-pHluorin (8). While it cannot be stated with certainty whether the diffusing pHluorins are components of multimolecular clusters or represent single molecules, the relatively high rates of diffusion argue against a cluster hypothesis. Second, pHluorins have been used to differentiate between proteins that reside on the plasma membrane and recently fused proteins (7,9). After bleaching or enzymatically removing the plasma membrane-resident pHluorins (synaptobrevin or synaptotagmin constructs), the kinetics of vesicle recycling and pHluorin movement were investigated. Both studies found that stimulation was followed by the endocytosis of a mixture of recently exocytosed and 'older' (membrane-resident) molecules. This result suggested that the vesicle structure was lost upon fusion, with the recently exocytosed molecules diffusing, mixing with the pool of membrane-resident pHluorins, and being subsequently endocytosed as mixed molecular assemblies. However, it cannot be stated with

certainty whether both 'old' and 'new' vesicles were separately endocytosed in the boutons, or whether mixed vesicles were taken up, as both of the paradigms would provide identical fluorescence recordings. Thus, one may tentatively conclude that, while an alternative hypothesis cannot be completely excluded, several pHluorin-tagged molecules escape from fusing vesicles and mix with a membrane-resident pool of molecules.

The information on the behavior of native (untagged) proteins is relatively scarce. At least one synaptic vesicle component, synaptotagmin, was observed to be organized in clusters in the plasma membrane in studies using diffraction-unlimited stimulated emission depletion (STED) microscopy (10). Synaptotagmin formed clusters of ~90 nm in diameter, both at rest and after depolarization, suggesting that the vesicle components may remain to some extent clustered during recycling. The same phenomenon was observed when investigating synaptotagmin in early endosomes [derived from the neuroendocrine cell line PC12, (11)]. These results, coupled with the fact that the distribution of some pHluorin-tagged proteins in the plasma membrane may not be particularly linked to synaptic boutons [and therefore they may not be optimal reporters for synaptic vesicle protein distribution, (8)], raise doubts on whether native proteins behave in a similar manner – i.e. whether native synaptic vesicle proteins do diffuse out of boutons upon stimulation, and whether their molecules mix upon endocytosis.

We have decided here to investigate this issue. While most endocytotic probes (such as the styryl FM dyes) are lost from synaptic vesicles upon exocytosis, the vesicle material can be labeled with antibodies recognizing the intravesicular domains of vesicle markers, such as synaptotagmin (10,12). The antibodies do not interfere with vesicle recycling, and are not lost during exocytosis (12,13), allowing thus an investigation of native protein behavior. We suggest here that the native proteins diffuse and mix only to a limited extent. We found that vesicle material diffuses out of boutons and into axonal areas only upon strong (unphysiological) stimulation; under moderate stimulation conditions, no diffusion was observed. Second, by taking advantage of the higher resolution of STED microscopy, we detected virtually no mixing of vesicle components upon repeated recycling. Finally, we also compared pHluorin-tagged and untagged proteins, and found their distributions in the plasma membrane to be different, with the native proteins forming clearly defined clusters while the tagged molecules were widely dispersed.

Results

Definition of the vesicle pools under investigation

To first define the working conditions, we quantified the amount of vesicle protein found fused onto the plasma membrane (surface pool) and in the recycling

pool of vesicles. We either exposed the cultures to anti-synaptotagmin antibodies on ice, in the absence of stimulation (surface pool), or at room temperature, using a stimulation paradigm known to recycle essentially all of the recycling pool vesicles (14), 600 action potentials (APs) delivered at 20 Hz. As a control, neurons were fixed and permeabilized, and the total vesicle pool was immunostained. Unsurprisingly, the recycling pool is substantially larger than the surface pool (Figure 1A); quantification of the fluorescence amounts indicated that ~19% of all synaptotagmin is present on the surface, while the recycling pool contained ~53% of synaptotagmin (Figure 1C). The surface pool value is in agreement with the percentages observed with pHluorin molecules [15–24% for synaptobrevin (6,8), ~8% for synaptophysin (8), ~22% for synaptotagmin (9), although only ~2% for vGlut1 (15)]. Our value for the recycling pool is higher than one obtained before [~20%, (16)], but it has to be noted that our recycling pool labeling paradigm necessarily also labeled the surface pool, which had gone undetected in the previous estimate, which was obtained by electron microscopy. Estimates from pHluorin studies, in which both the internal recycling pool and the surface pool were analyzed together as one recycling pool, are essentially identical to our estimate (17).

Of course, the recycling pool needs not be completely stable, and may mix with the reserve pool (with repeated stimulation triggering release also of reserve vesicles, see below), so that the total pool of vesicles that can be mobilized upon repeated stimulation might be even larger. Note that the epitope availability is different for live labeling and for the fixed preparations, so the real numbers may be somewhat different.

To define the size of the readily releasable pool (or the vesicles known to recycle under moderate, physiologically relevant stimulation), we stimulated the nerve terminals using 40 AP delivered at 20 Hz (18). To be able to differentiate the internalized vesicles from the surface molecules, we resorted to FM 1-43 labeling followed by photoconversion (photooxidation) of the dye (16,18), which transforms the fluorescence label in a dense precipitate, visible in electron microscopy (Figure 1B). Approximately 19% of the vesicles were labeled (Figure 1C). Interestingly, the surface pool of vesicle material is thus almost equal to the readily releasable pool; the two may interchange, as indicated by the fact that the surface pool of molecules is rapidly (2–5 min) internalized after surface labeling (19).

Synaptotagmin escape from synaptic boutons

To investigate the mobility of synaptic material after exocytosis, we labeled the surface pool of synaptotagmin using a fluorescently labeled anti-synaptotagmin antibody and then allowed the vesicles to endocytose for 20 min at room temperature [a time period after which less than 20% of the surface molecules persist on the surface, (19)]. Alternatively, we allowed the vesicle material to recycle repeatedly at physiological temperature (37°C), under

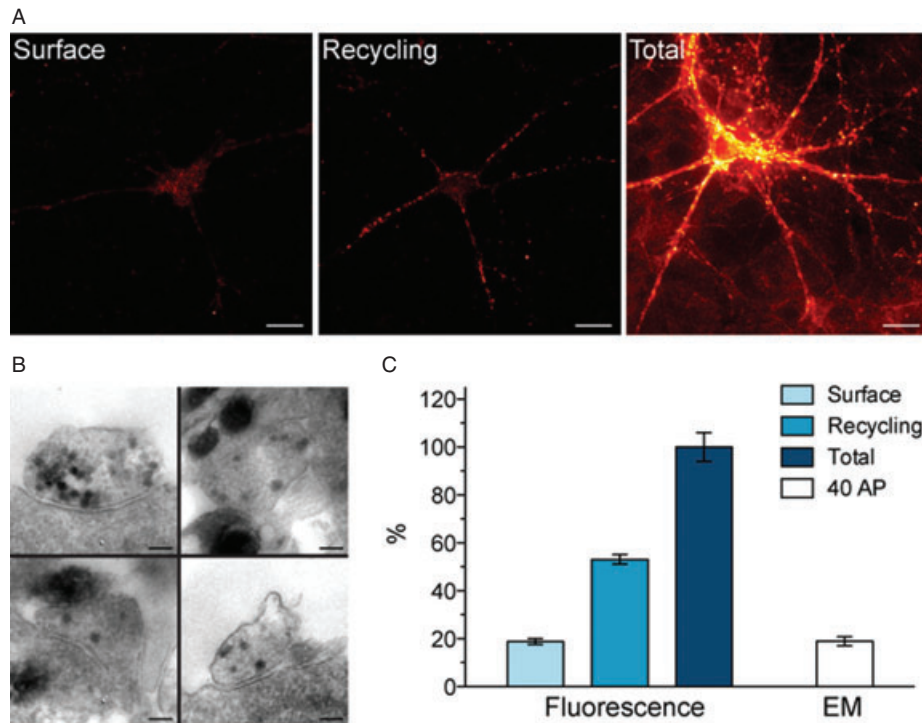


Figure 1: Definition of the vesicle pools under investigation.

A) The surface pool of synaptotagmin was immunolabeled using an anti-synaptotagmin monoclonal antibody (labeled with the dye Atto 647N; left panel). The recycling vesicle pool was labeled by 600 AP delivered at 20 Hz in the presence of the antibody (center). Finally, the full complement of synaptotagmin was immunostained after fixation and membrane permeabilization (right panel). Scale bar = 20 μ m. B) The vesicle pool recycling after a 40 AP (20 Hz) stimulus was investigated by FM 1-43 uptake followed by photoconversion and electron microscopy. Note the dark (labeled) vesicles. Scale bar = 100 nm. C) Quantification of the pool sizes, as percentage of all vesicles. Data are presented as mean \pm SEM ($n = 3-5$ experiments).

normal culture activity, for 1 h, thereby allowing for any potential integration of the recently labeled vesicles in the recycling or reserve pools. We then monitored the amount of fluorescence in boutons and in interbouton areas before, during and after electrical stimulation. As indicated in Figure 2A, no substantial changes were noted during stimulation using 40 AP (20 Hz), an impression confirmed by quantifying the amount of fluorescence in interbouton areas expressed as a percentage of the fluorescence in the neighboring boutons (Figure 2B). No difference was observed between vesicles incubated shortly at room temperature or for prolonged periods of time at 37°C. The result is somewhat surprising, as pHluorin-tagged molecules have been observed to escape boutons under such stimulation (8). Moreover, a significant escape from the boutons during 40 AP stimulation was observed even with a much less pH-sensitive fluorescent tag (mRFP; 8), in an approach that was independent of the pH sensitivity of the reporter, and thus closely followed our detection paradigm. The imaging conditions were such that background spots (single antibodies) could be detected (Figure S1 and Movie S1).

Stronger stimulation is predicted to eventually result in the spread of synaptic material in the intersynaptic space, as observed in different assays, not only relying on tagged proteins [e.g. (20)]. A 600 AP stimulus did increase the proportion of axonal synaptotagmin, although the increase lagged by ~ 4 seconds after the start of the stimulus (Figure 2B). Again, no difference was observed between vesicles incubated for different periods of time after labeling. We conclude that, while the escape of vesicle material

from boutons is undeniable, it seems to be restricted to relatively strong stimuli. Therefore, one may expect that, at least under moderate stimulation, the synaptic vesicles recycle locally.

Mixing of synaptotagmin molecules

We next attempted to address the question of whether the vesicle molecules intermix during recycling. Ideally, one would label vesicle molecules in two different vesicle populations with different fluorescent markers, and would then investigate the composition of the single synaptic vesicles after recycling. We pursued this direction by labeling different vesicles with anti-synaptotagmin antibodies coupled to two different fluorescent molecules (Oyster 550 and Atto 647N), and then investigated the colocalization of the dyes. Monitoring the two molecules in confocal microscopy is difficult, as the imaging resolution is not sufficient – at least one of the molecules should be studied with high resolution. We therefore turned to STED microscopy (10), where the excitation beam is overlapped with a second, doughnut-shaped beam, which quenches the excited molecules by stimulated depletion. As a result, fluorescence is generated selectively in the center of the excitation spot, where the quenching beam has its lowest intensity, close to zero. The resulting focal area is narrower than the diffraction limit, and therefore provides higher resolution. Our set-up (see *Materials and Methods*) provides a resolution optimum of $\sim 70-90$ nm for the Atto 647N dye, as tested by imaging single antibodies on coverslips. However, as the Z-resolution of the technique is only of $\sim 500-600$ nm, we fixed and embedded the preparations in a material that allows for efficient

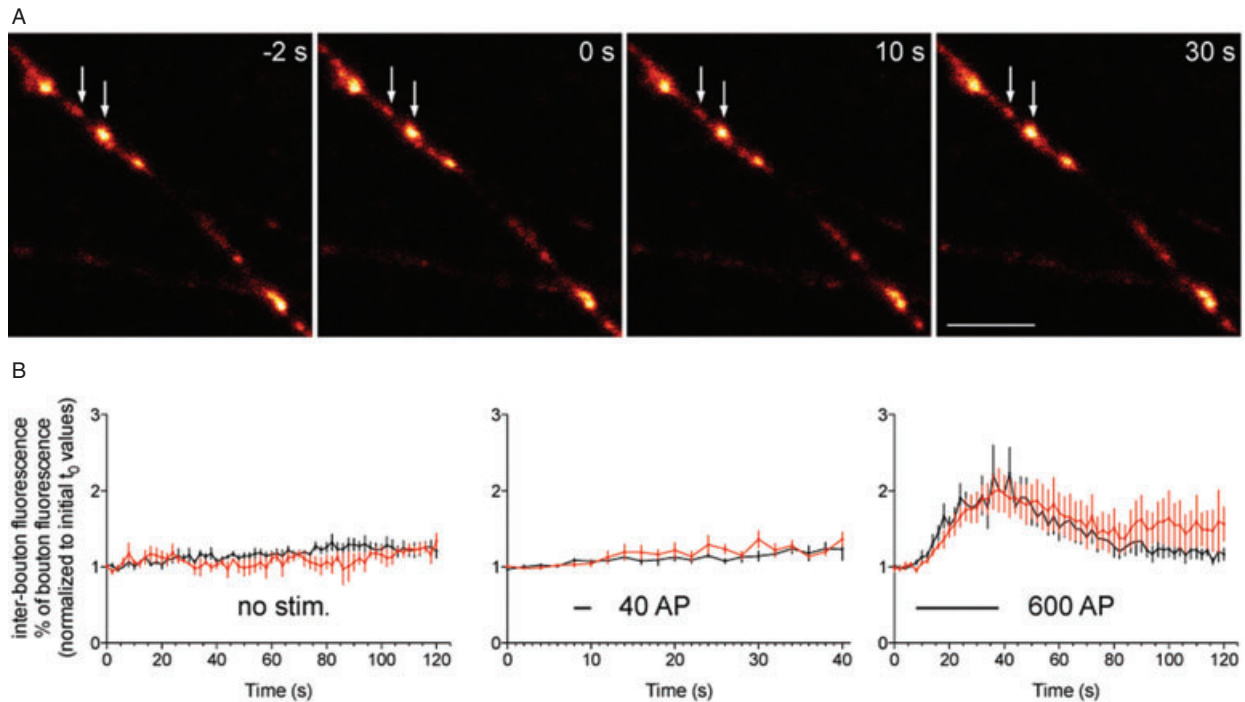


Figure 2: Escape of synaptotagmin molecules from synaptic boutons. A) The surface pool of synaptotagmin was labeled as above (using a synaptotagmin antibody coupled to Atto 647N), allowed to internalize for 20 min at room temperature, before confocal (conventional) imaging. The panels indicate several synaptic boutons at different time-points after a stimulus of 40 AP at 20 Hz. Scale bar = 5 μ m. B) Analysis of the amount of synaptotagmin fluorescence in interbouton areas. The fluorescence in interbouton areas was expressed as the percentage of the fluorescence in two manually selected neighboring boutons (example indicated by arrows in A). To allow for a comparison of the change in signal over time, the curves were normalized to their initial values. Note that no change is observed under 40 AP stimulation (center), while an increase in the amount of synaptotagmin material in axonal areas takes place upon 600 AP stimulation (right panel). Black traces, preparations allowed to recycle vesicles at room temperature for 20 min. Red traces, preparations allowed to recycle vesicles for 1 h at 37°C. Traces represent the mean of 4–6 independent experiments \pm SEM. The numbers of experiments/interbouton spots analyzed were preparations incubated at room temperature (black traces): no stim 6/90, 40 AP 6/181, 600 AP 6/111; preparations incubated at 37°C (red traces): no stim 4/63, 40 AP 4/105, 600 AP 4/73.

stimulated depletion [melamine, (21)], before processing them in thin (80–90 nm) sections (Figure 3A,B).

We used several labeling paradigms to test the intermixing of different molecules. We incubated the preparations in the presence of Oyster 550-coupled anti-synaptotagmin antibodies, under no stimulation conditions, under 40 AP stimulation, or with a recycling pool-releasing 600 AP stimulus. Antibody wash-off was followed by a resting period (20 min at room temperature), and a new round of labeling, using the same protocols in the presence of Atto 647N-coupled antibodies. As a positive control, cultures were simultaneously labeled with both antibodies; as a negative control, the surface pool was marked with Oyster 550, the vesicles were allowed to recycle (internalize), and the cultures were then fixed and surface-stained with Atto 647N. As a percentage of the synaptotagmin molecules is always on the surface (see above), one would expect some colocalization of the two labels even in the negative control. We estimate that on average \sim 5–6 antibodies are labeling one fused vesicle (Figure S3).

We processed the preparations in thin sections and investigated the Oyster 550 label by confocal imaging, and the Atto 647N label with STED optics. The overall 80–90 nm resolution in all dimensions for the STED channel (70–90 in X – Y , and 80–90 in Z), coupled with the relatively sparse spacing of the labeled vesicles, allowed for identifying what appear to be single Atto-labeled vesicles (Figure 3C; see also STED spot dimensions in Figure 3D). The confocal X – Y resolution is clearly insufficient to distinguish single vesicles in the Oyster 550 channel (full width at half maximum, FWHM, of 267 ± 2.9 nm in 194 single spots investigated); however, the relatively sparse labeling obtained by increasing the Z -resolution allowed us to correlate the two signals with relatively high precision.

We next quantified the amount of overlap between the STED and the Oyster signal. The images were filtered using an unsharp filter (which subtracts a blurred version of the image from the original image, therefore rendering a sharper, largely background-corrected, version of the original image), and an automatic threshold

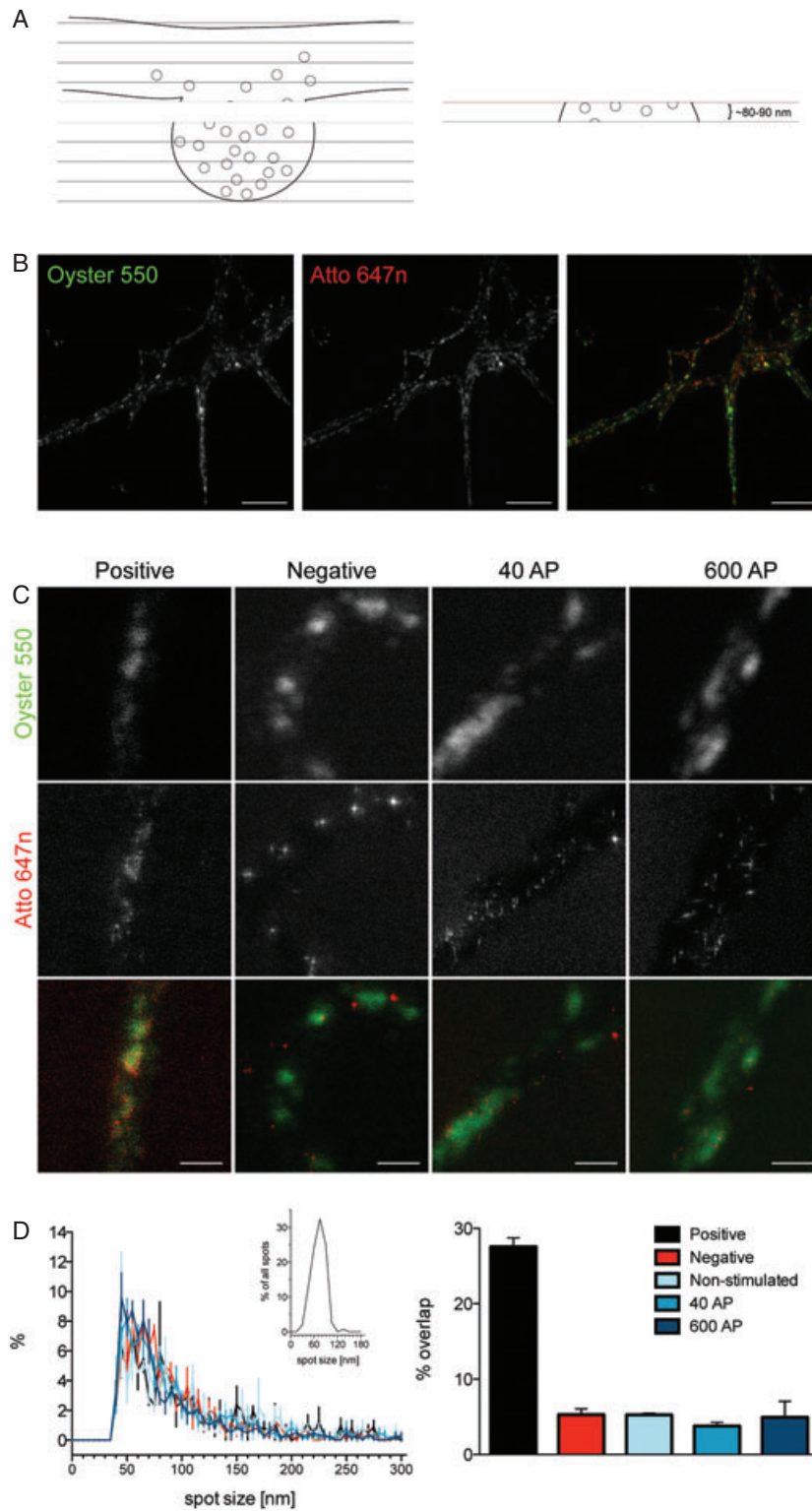


Figure 3: Intermixing of synaptotagmin molecules.

A) Schematic representation of the experiment. Labeled cultures were embedded in plastic material, and processed in 80–90 nm sections. B) Overview images of a thin section through a neuron labeled with both synaptotagmin Atto 647N- and Oyster 550-coupled antibodies. Scale bar = 20 μ m. C) Higher resolution images of labeled boutons. Positive column, double-labeled preparations (positive control, incubated simultaneously with both antibodies). Negative column, neurons were surface labeled using Oyster 550-labeled antibodies, allowed to recycle the vesicles at 37°C, followed by fixation and surface staining with unlabeled synaptotagmin antibodies/Atto647N-labeled Fab secondaries (negative control). Forty and 600 AP column, preparations labeled by 40 or 600 AP stimulation in the presence of the Oyster 550-labeled antibody, followed by wash-off and labeling by 40 or 600 AP stimulation in the presence of the Atto 647N-labeled antibody. Scale bars = 1 μ m. D) Left panel, histogram of the spot size in the STED images. Inset indicates the resolution of the microscope, determined from the measurements of single background spots. Right panel, quantification of the colocalization expressed in percentage of the area of Oyster 550 signal overlapping with Atto 647N spots. Data are presented as mean \pm SEM ($n = 3$ independent experiments). The numbers of spots analyzed for the size distributions have been 255, 80 and 60 (positive control); 160, 226 and 217 (negative control); 103, 424 and 86 (non-stimulated); 204, 252 and 332 (40 AP); 297, 321 and 372 (600 AP). The numbers of axonal areas studied for the overlap analysis are 17, 13, 18 (positive control); 28, 14, 19 (negative control); 27, 23, 16 (non-stimulated); 57, 44, 63 (40 AP); 50, 44, 53 (600 AP). An average from multiple overlapping spots has been obtained from each area investigated.

(set to a value 1.5-fold higher than the mean intensity of the region under investigation) was used to identify the fluorescent spots in both channels. The area of the Oyster signal covered by STED spots was determined, and was around 25–30% for the positive control

(double-simultaneously-labeled vesicles). With the Oyster spot size (confocal) being substantially larger than the STED spot size, the result is entirely expected. For the negative control, a substantially lower overlap was obtained (~5%; $p < 0.01$, t -test). For all other labeling paradigms,

we obtained overlap values similar to that of the negative control (Figure 3D). Interestingly, no substantial overlap was observed even when stimulating the repeated release of the recycling pool (Figure 3C). Atto 647N signal was relatively abundant (~40% more abundant than for the 40 AP stimulation when quantifying the total intensity of single neuronal sections; three independent experiments were analyzed, with 9–12 neurons investigated in each experiment). It colocalized poorly with the Oyster 550 signal. This indicates that the second 600 AP stimulus did release a number of vesicles, which had not recycled on the first stimulus (and therefore escaped Oyster 550 labeling), and suggests that these vesicles had been then endocytosed independently from the Oyster 550-labeled molecules. Thus, we obtained basically no evidence for a mixing of fluorescently labeled synaptotagmin molecules, under several different stimulation paradigms.

In a second approach, we used two-color STED (22) to investigate the same issue. We labeled the preparations using the same protocols as above (using an antibody coupled to Atto 590 rather than Oyster 550). We have then investigated the samples using a two-color STED set-up, as described in *Materials and Methods* (Figure 4A–D). The resolution of the system is high in both channels (FWHM of ~60 nm for Atto 590 and ~70 nm for Atto 647N; Figure 4E). As both imaging channels are of comparable resolution, one can use more direct analysis methods here, such as Pearson's correlation coefficient calculations, rather than the overlap analysis.

As correlation coefficients are strongly dependent on the imaging noise and labeling conditions, a maximum (control) correlation coefficient must be obtained before interpreting the data [see an example from our own work (23), Figure 1G]. To identify the maximum correlation we can expect, we stained the surface pool of synaptotagmin with Atto 647N-coupled antibodies, and we poststained the antibodies with Atto 590-coupled secondaries. The two-color images (Figure S4) correlate well, as expected, and provide a numeric correlation coefficient of ~0.32.

We then calculated the correlation coefficients for the experimental images (Figure 4F), and expressed them in percent of the maximum correlation. As in the previous experiments (Figure 3), no significant increase in signal colocalization (over the negative control) was observed upon stimulation, even in the 600 AP protocol ($p > 0.05$, t -tests). Thus, using two-color STED, we again obtained no evidence for a mixing of fluorescently labeled synaptotagmin molecules.

Surface clusters of synaptic vesicle proteins

We have previously suggested that synaptotagmin forms clusters on the plasma membrane (10); whether other synaptic proteins form similar clusters is still an open issue. To test this experimentally, antibodies directed against the intravesicular domains of the proteins are

required. While those against synaptotagmin have been available for more than a decade, we have only recently obtained two antibodies against the intravesicular domains of synaptophysin and the vesicular GABA transporter (VGAT). We live-stained hippocampal cultures with these antibodies (same as for synaptotagmin surface staining, see above), then fixed them and immunostained the surface molecules with Atto 647N-coupled secondary Fab fragments (to enhance the signal by secondary detection). STED images of the preparations show that both synaptophysin and VGAT form clusters, similar to those of synaptotagmin (Figure 6A, upper panels).

The diffusion of pHluorins from synaptic boutons (see introduction) suggests that they may be organized differently in the membrane. To test this, we investigated three GFP-tagged vesicle proteins, synaptobrevin-pHluorin, synaptophysin-pHluorin, and to test whether the effects we found were due exclusively to the pHluorin tag, a citrine-tagged variant of synaptotagmin (see *Materials and Methods* for details). We live-stained cell cultures expressing the different GFP-tagged variants using antibodies directed against the GFP moiety. We used immunostaining, rather than GFP imaging, for both conceptual and technical reasons. First, one should use the same procedure for investigating GFP-tagged and untagged proteins: one should investigate both by immunostaining, rather than one by immunostaining and one by GFP fluorescence.

Second, one cannot use the GFP fluorescence to investigate selectively the surface pool of molecules. We have not succeeded in imaging pHluorins in live STED microscopy; imaging pHluorins by STED in fixed cells is impossible, as in fixed cells the pH gradient of the vesicles is neutralized, and therefore one cannot rely on pHluorin quenching to eliminate the fluorescence of the internal pool of molecules.

We found that, interestingly, the GFP-tagged proteins were much less clustered than the native proteins (Figure 6A, lower panels). It is also important to note that the difference observed between the stainings was hardly visible when only confocal (conventional resolution) images were investigated (Figure 6A, left panels), indicating that this phenotype could not have been noticed in previous investigations using conventional microscopy.

Quantification of the protein clustering

We have first analyzed the size of the clusters (spots) formed by the different proteins. Line scans were drawn on the individual spots, and the FWHM was obtained from fitting Lorentzian curves to the scans (10). As indicated in Figure 5B, the cluster size for native proteins was around 100 nm. Spot size was much higher (typically larger than ~200 nm) for synaptobrevin-pHluorin and synaptophysin-pHluorin, and somewhat intermediate for synaptotagmin-citrine (Figure 5B). The difference between native and tagged proteins does not seem to be driven exclusively by the overexpression of the protein, as

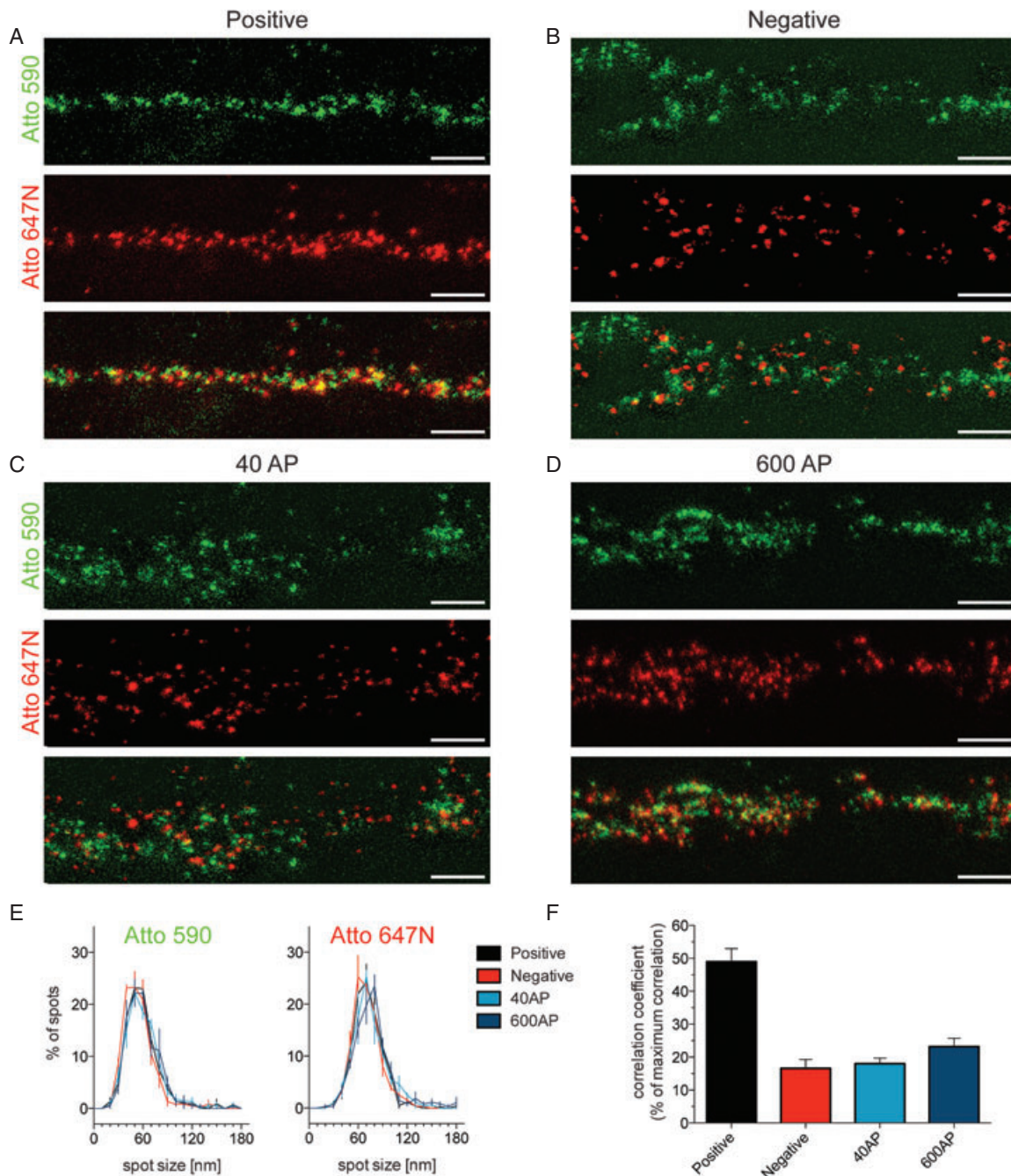


Figure 4: Two-color STED analysis of molecule intermixing. A–D) Preparations were labeled as in Figure 3, and investigated by two-color STED microscopy, using antibodies coupled to Atto 590 and Atto 647N. Scale bar = 1 μ m. E) STED spot sizes (FWHM) in the different conditions. Approximately 100 spots were analyzed per condition in each experiment (three independent experiments). Error bars indicate SEM. F) The Pearson's correlation coefficients were calculated for axonal areas (excluding background). The values are presented as percent of maximal correlation obtainable under our imaging/analysis conditions. Bars show mean \pm SEM. Between 47 and 66 axonal areas were analyzed per condition, from three independent experiments each.

the expression level did not correlate well with the ability to form distinguishable clusters (Figure S5).

This analysis deals exclusively with plasma membrane clusters (spots), and thus ignores the larger areas

where the signal is more diffuse. To obtain a more comprehensive view of the protein distribution, we pursued an autocorrelation analysis (see model in Figure 6A). In this approach, a STED image was superimposed onto itself, and the superimposed image was horizontally

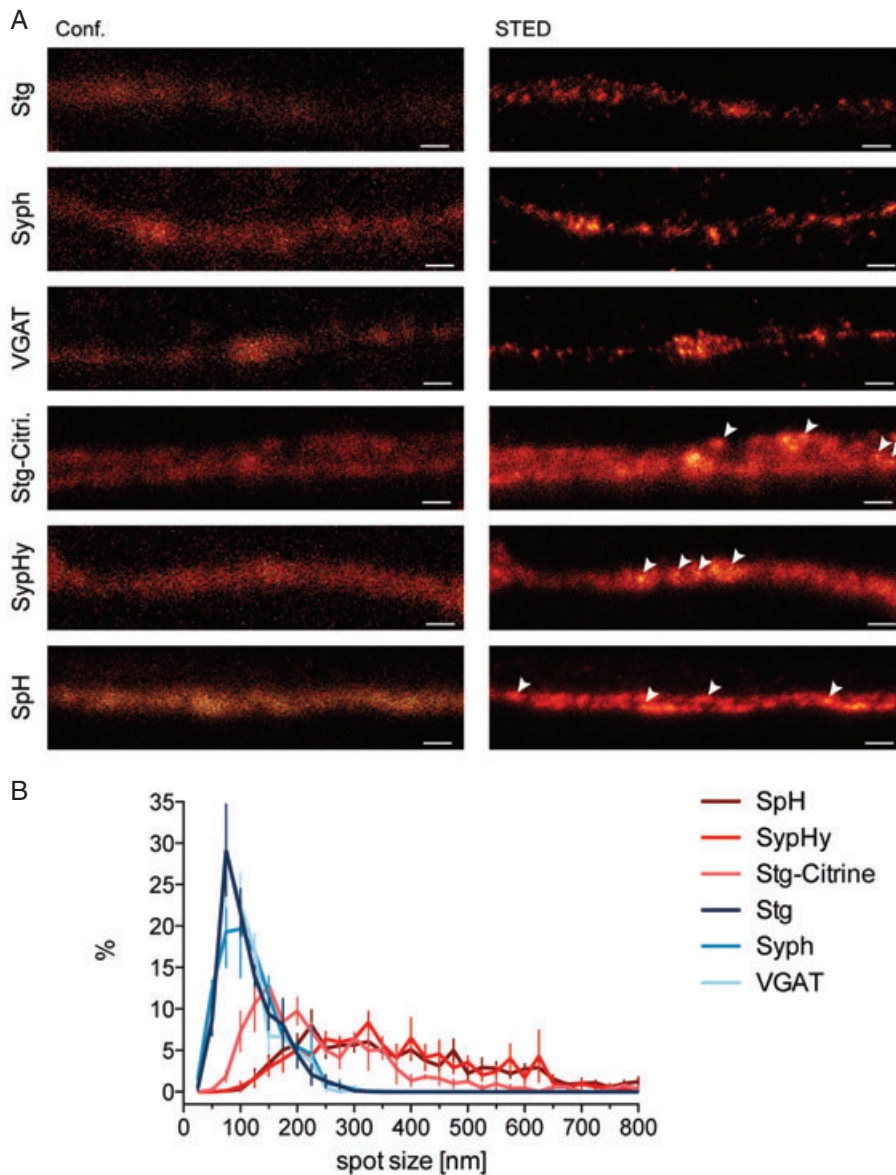


Figure 5: Plasma membrane localization of native and GFP-tagged synaptic proteins. A) STED (right panels) and confocal (left panels) images of hippocampal axons live-stained for synaptotagmin (Stg), synaptophysin (Syph), the vesicular GABA transporter (VGAT), or synaptotagmin-citrine (Stg-Citrine), synaptophysin-pHluorin (SyphHy) and synaptobrevin-pHluorin (SpH). Note that all confocal images are comparable. Clear spots/clusters can be observed in the STED images of the endogenous synaptic proteins, but not in the overexpressed ones. Scale bar = 500 nm. Antibodies against the respective proteins were used for the untagged molecules; antibodies recognizing GFP were used for the tagged proteins. B) Histogram of spot sizes. Spots were manually selected, and horizontal line scans were automatically generated. The full width at half maximum for the spots was obtained from Lorentzian fits to the line scans, and is presented in the figure as spot size. The histograms were normalized to the total number of spots. Data are presented as mean \pm SEM of 3–10 independent experiments. Several images were taken from three to six neurons for each independent experiment. The distributions of the tagged proteins are significantly different from those of the native proteins (Kolmogorov–Smirnov tests, $p < 0.05$).

shifted, pixel-by-pixel, calculating the Pearson’s correlation coefficient between the image and the superimposed copy at every shift. The image initially correlates perfectly to itself (coefficient of 1), and the correlation becomes poorer as the shift increases. As the model indicates, an image with small spots loses correlation sooner than one with larger spots (as smaller pixel shift is sufficient to make small, but not large, spots lose the overlap with themselves). Applying this method to all imaged proteins indicated that the autocorrelation dropped faster for the native proteins than for the tagged proteins. As the initial drop in correlation (upon the first pixel shift) is because of the random single-pixel noise of the images, we have investigated the same curves normalized to the 1-pixel shift position. As the initial shift, of broadly the same size as the protein clusters (~ 100 – 200 nm, or ~ 10 – 20 pixels), is the most relevant component of the autocorrelation

traces, we have also displayed it separately (Figure 6B). As the curves can be approximated by linear equations in this shift interval, we performed linear regressions for all traces (Figure 6C). The slopes for the GFP-tagged proteins were significantly less steep for synaptobrevin- and synaptophysin-pHluorin than for all of the native proteins, while the behavior was intermediate for synaptotagmin.

As a second measure of the protein distribution, we turned to an investigation of pixel intensities. In each image analyzed, we determined the axonal area and generated a histogram of the pixel intensities within it. For images where the signal is concentrated in a few spots, the histogram is dominated by low intensity values (see example in Figure 6D, top panels). In contrast, in images with diffuse signal, the histogram is broader, containing fewer low intensity values, and more pixels of intermediate

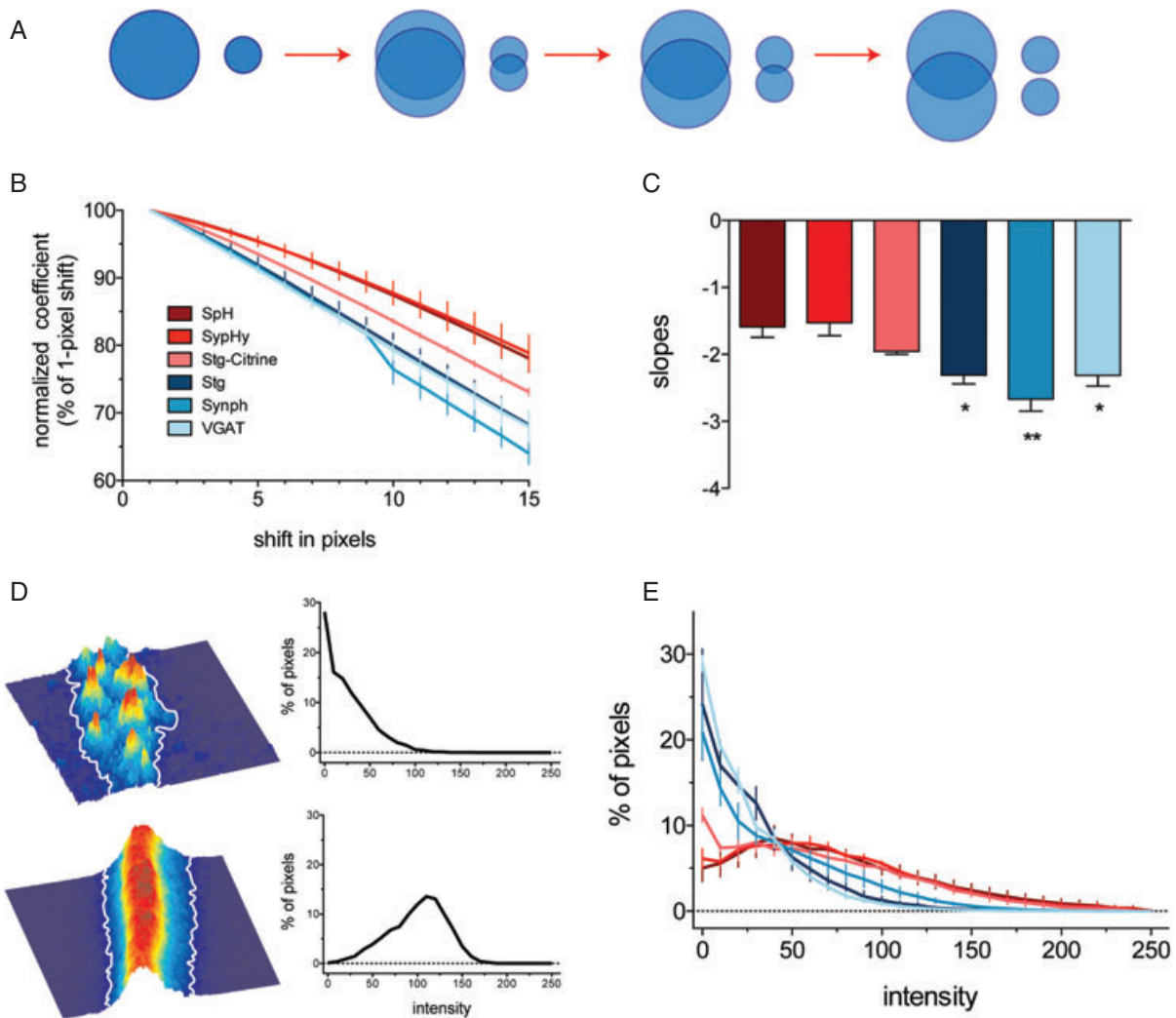


Figure 6: Evaluation of the protein clustering. A–C) Autocorrelation analysis. A) Simple representation of the autocorrelation analysis. Spots (images) are duplicated and superimposed; their perfect correlation with themselves gives a Pearson's correlation coefficient of 1. Shifting one of the superimposed images reduces the correlation. Note that large spots tend to correlate (superimpose) with themselves even at high pixel shifts, while the small ones lose the correlation rapidly. B) We performed an autocorrelation analysis for the different proteins investigated. To avoid differences because of uneven levels of noise in the analyzed images, we normalized the curves to the value of the first pixel shift (which represents the drop upon the first pixel movement, a value strongly dominated by the noise difference between neighboring pixels). We display the values from the 1st to the 15th pixel shift. As pixel size is 9.47 nm, the 15-pixel shift approximates the size of a large protein cluster, or ~150 nm. Data are presented as mean \pm SEM from three to five independent experiments. C) Linear regression fits were performed to the curves in (B) and the slopes were calculated. The slopes are steeper for the native proteins (significantly steeper than for synaptophysin or synaptobrevin-pHluorin; ** $p < 0.01$; * $p < 0.05$, one-way ANOVA/Newman–Keuls multiple comparison test), indicating that the signal in these images is more 'spotty'. Tagged synaptotagmin has an intermediate behavior. D and E) Intensity histogram analysis. D) STED examples of live staining. Top panel: 3D view of an example axonal fragment. The axonal area (delimited by the white line) consists of a few bright spots on a lower background. Bottom panel: 3D view of an axon in which the signal is diffuse/evenly distributed. The histograms of pixel intensity presented in the panels (right) indicate that in the first case low pixel intensities dominate, while in the second case the moderately bright pixels are much more frequent. E) Histograms for the proteins of interest were generated. Mean \pm SEM from three to five independent experiments are presented. Note the substantial difference between the native and tagged distributions, which confirms the visual impression that the tagged proteins are more diffusely organized.

brightness (see example in Figure 6D, lower panels). As indicated in Figure 6E, the histograms for the native proteins were all dominated by low (0–25 AU) pixel values, while this was not the case for the GFP-tagged variants.

We conclude that, while several native synaptic vesicle proteins are found in relatively small clusters on the plasma membrane (on the size of fused vesicles), GFP-tagged variants are much more broadly and diffusely distributed.

Discussion

By investigating native synaptic vesicle markers via antibody labeling, we found that several are clustered on the plasma membrane (although GFP-tagged variants were not). Native synaptotagmin required substantial stimulation to diffuse out of synapses, while it seemed to recycle locally at moderate stimulation. Moreover, repeated recycling in the presence of different labels provided no evidence for intermixing of native synaptotagmin molecules.

The previous evidence on the behavior of synaptic vesicle components in the plasma membrane has been derived almost exclusively from the study of pHluorin-tagged molecules. Currently, it cannot be doubted that they are virtually perfect reporters of exocytosis. Transfected synaptic boutons still take up and release membrane markers such as styryl (FM) dyes (6–9,24,25), with kinetics identical to the untransfected boutons. Moreover, the change in pHluorin signal upon exocytosis also perfectly parallels the kinetics expected from the release of styryl dyes. However, our results indicate that GFP-tagged variants of synaptic vesicle proteins are a poor substitute for native proteins in terms of plasma membrane localization, as they have a much more diffuse signal, not restricted to small clusters. The effects were not linked exclusively to pHluorin, as the (similar) GFP-variant citrine also disturbed the protein behavior. While native synaptobrevin could not be analyzed, because no antibodies against its intravesicular domain are available, it is possible that it behaves in a similar manner to native synaptotagmin and synaptophysin, with which it has been observed to form detergent-resistant complexes (26) that may recycle as whole units. Moreover, synaptobrevin is present at very low levels in the plasma membrane, as observed by biochemical means [e.g. (27)], while synaptobrevin-pHluorin is substantially expressed here (6,8).

Our observations would have hardly been possible without high-resolution microscopy, although doubts as to the appropriate location of at least certain pHluorins have already been expressed (8). Our results impact on a number of studies using pHluorins, especially those analyzing the dynamics of endocytosis. It is highly unlikely that the localization of pHluorins in the plasma membrane has any effects on exocytosis and the subsequent pHluorin brightness increase; however, if the pHluorins diffuse after exocytosis instead of remaining in (or being integrated into) vesicle protein clusters, pHluorin endocytosis may function with different dynamics than the endocytosis of native proteins. Several studies have investigated detailed pHluorin endocytosis kinetics, even on the single-vesicle level [e.g. (28,29)]. The tagged molecules are occasionally observed to endocytose with rapid kinetics, with some being rapidly internalized (28), and with others retrieved more slowly, or even in two different steps (29), in what is a rather confusing model in view of the clustered nature of native proteins. It has already been suggested that the change in signal originally associated with rapid

endocytosis may be an artifact of the diffusion of the tagged molecules from the fusion site (8) – a point which is in strong agreement with our results. The diffusion of pHluorins easily provides an explanation for the other phenotypes as well, with the normal vesicular recycling mechanisms only able to capture a fraction of the pHluorins from a fused vesicle. The remaining ones may either persist as stranded molecules, or may be slowly internalized, with what may represent abnormal kinetics. Interestingly, other tools, not dependent on protein overexpression, such as FM (styryl) dyes or quantum dots (30–34) have argued for more than a decade for modes of rapid recycling in which no diffusion of the proteins from the vesicle can be expected.

Our results are in agreement with the previous findings on the internalization of synaptic vesicle components performed by electron microscopy of preparations frozen at different time-points after massive stimulation [1 AP delivered in 4-aminopyridine, (20)]. A fraction of the vesicles were taken up within a few seconds after exocytosis, in what likely represents preassembled clathrin-coated pits. Little vesicle intermixing can be expected in this situation, with the material taken up consisting of vesicle components present on the surface before the start of stimulation. Larger pits were later observed, which seemed to collect various vesicular components, beside smaller pits collecting what appeared to be single vesicle units. Representing bulk endocytosis, the large pits presumably collected molecules indiscriminately, which may have resulted in some mixing of vesicle components. However, as bulk endocytosis only takes place upon strong stimulation in the particular preparation [frog neuromuscular junction; see Ref (35)], one may tentatively conclude that under moderate stimulation synaptic vesicles could be retrieved without substantial mixing of components. This was to some extent confirmed by Wienisch and Klingauf (7) also in the hippocampal culture, as a 40 AP stimulus only retrieved surface-resident pHluorin molecules, with essentially all recently exocytosed molecules remaining stranded on the plasma membrane – and thus no mixing of the vesicle components.

The synaptotagmin clusters in the plasma membrane seem to consist of several copies (10). It is, however, difficult to state whether they contain the entire complement of a synaptic vesicle [more than 10 copies, (27)] or whether they represent only vesicular fragments. Most clusters are substantially brighter than single antibodies (10), but the tight packing of molecules in a vesicle (or fused vesicle) would at any rate preclude the labeling of all copies by antibody binding due to steric hindrance. Thus, as it cannot be currently excluded that the clusters represent only parts of vesicles, it is still in principle possible that several vesicle clusters are collected during endocytosis into single vesicles, which opens the possibility that recently exocytosed and membrane-resident molecules would intermix. It has been thoroughly established that both recently exocytosed and membrane-resident pHluorin-tagged

components can be taken up after stimulation (7,9). However, while these studies concluded that the material was endocytosed in single vesicles composed of intermixed molecules, an alternative explanation may be possible, as indicated in the introduction – that separate vesicles consisting of different types of molecules are taken up in the same boutons (with our experiments being in better agreement with the second hypothesis, Figure 3).

Our results still do not show that synaptic vesicle molecules remain grouped upon exocytosis – it cannot be excluded that different molecular clusters separate, or that several proteins are lost from the vesicles. However, at least for synaptotagmin, the intermixing of components from different vesicles seems limited. Also, the clustering of molecules appears to be a paradigm for all synaptic vesicle molecules tested to date.

Materials and Methods

Molecular biology

Both synaptobrevin and synaptophysin fused to pHlourin were generous gifts from Professor Leon Lagnado (MRC). The synaptotagmin-citrine construct was generated in two steps. First, the citrine fluorophore gene was obtained from the laboratory of Professor Stefan Hell (Max Planck Institute for Biophysical Chemistry), with permission (Material Transfer Agreement) from the original producer of the clone (Professor Roger Y. Tsien, Howard Hughes Medical Institute). Then, citrine gene was amplified using polymerase chain reaction (PCR) technique with the following oligos (forward: 5'-ATTACCGGTCGCCACCATGGTGAGCAAGGGCG-3' and reverse: 5'-TCGAGATCTGAGTCCGGACTTGACAGCTCGTC-3') and cloned into pEGFP-C1 (Clontech GmbH) at *AgeI* and *BglII* sites (Fermentas GmbH), thus replacing EGFP (termed pCitrine-C1). The full-length synaptotagmin I (a generous gift from Professor Reinhard Jahn, Max Planck Institute for Biophysical Chemistry) was amplified by PCR and cloned into pCitrine-C1 (oligos: 5'-ATTTAGATCTATGGTGAGTGCCAGTCATC3' and 5'-ATTTGGATCCTTACTTCTTGACAGCCAGC-3') at *BglII* and *BamHI* sites. All constructs, both gifts and self-created ones, were purified using an Endo-Free Maxi kit (Qiagen), and finally sequenced.

Primary hippocampal culture

Brains of newborn rats were removed and placed in cold HBSS (Invitrogen). Hippocampi were detached from cortex and incubated 1 h in an enzyme solution [in DMEM (Invitrogen), 2 mg cysteine, 100 mM CaCl₂, 50 mM ethylenediaminetetraacetic acid (EDTA), 25 units papain per mL of solution, with CO₂ bubbling, at 37°C]. The enzymatic solution was afterwards removed and replaced for 5 min with an inactivating solution (in 5% FCS-DMEM, 25 mg albumin and 25 mg trypsin inhibitor). Then, the hippocampi were triturated using a Pasteur pipette in complete-neurobasal medium [Neurobasal A (Invitrogen), supplemented with 20% B27 (Invitrogen) and 10% Glutamax-1 (Invitrogen), 20 units/mL penicillin and 20 µg/mL streptomycin (Roche-Diagnostics)]. Neurons were plated (12-well plate) on poly-D-lysine-(Sigma-Aldrich) coated coverslips, on a previously grown layer of astrocytes.

Neuronal transfection

Primary hippocampal neurons were transfected at 8–15 days *in vitro* (DIV). We employed the following transfection methods: Lipofectamine 2000 (Invitrogen), calcium phosphate (Promega GmbH) and Magnetofection (Oz Biosciences), according to manufacturer's instructions. When lipofectamine was used, the neuronal conditioned medium was saved and replaced by prewarmed complete-neurobasal (see above) medium. A mixture of 3.5 µg of DNA/7 µL of Lipofectamine 2000 in complete-neurobasal

medium was prepared as indicated by the manufacturer. After 25 min of incubation at room temperature, 100 µL of the DNA/lipofectamine solution was added per well and incubated for 4 h. Subsequently, neurons were washed once with prewarmed complete-neurobasal medium and left in the previously saved conditioned medium.

The calcium phosphate-mediated transfection was performed using the ProFection Mammalian Transfection System (Promega). Briefly, conditioned medium was saved and replaced with prewarmed complete-neurobasal medium. The DNA for two wells was prepared by adding 10 µg total DNA and 12.5 µL of CaCl₂ (2 M) into a final volume of 100 µL of nuclease-free water. While vortexing the CaCl₂/DNA solution, 100 µL of 2× HEPES-buffered saline (Promega GmbH) was slowly added, drop-by-drop. The final mixture was left at room temperature for 20 min, to allow crystal formation. Hundred microliters of the DNA-precipitate solution was added to each well and the neurons were incubated for 4 h. Neurons were rapidly washed 3×, followed by one final wash of 15 min (in the incubator) with calcium- and magnesium-free HBSS (Invitrogen). HBSS was finally replaced by a 1:1 mixture of conditioned: fresh complete-neurobasal media.

The transfection performed by the magnetofection system did not require any change of media. For each well, we mixed 5 µg of total DNA with 7 µL of NeuroMag in 100 µL of complete-neurobasal medium. The preparation was kept for 25 min at room temperature before adding it drop-by-drop to the neurons. The neurons were subsequently placed on top of a magnetic plate inside the incubator for 15 min. After this time the magnet was removed.

All cultures were used within 48 h after transfection, irrespective of the transfection method used. We observed no differences between the different transfection methods regarding protein expression and distribution.

Immunocytochemistry

All incubations were performed in Tyrode buffer containing 124 mM NaCl, 5 mM KCl, 2 mM CaCl₂, 1 mM MgCl₂, 30 mM glucose and 25 mM HEPES (pH 7.4), unless otherwise described. For experiments investigating the surface distribution of different proteins, the neurons were rapidly exposed to the antisynaptic vesicle protein antibodies for 5 min in ice-cold Tyrode. The following antibodies were used: monoclonal anti-GFP 3E6 from Molecular Probes (Invitrogen), monoclonal antibody against the luminal (intravesicular) domain of synaptotagmin I, CL 604.2, from Synaptic System (Göttingen), polyclonal anti-synaptophysin serum, G96, and a polyclonal anti-GABA transporter serum, R24; the polyclonal antibodies were kind gifts from Professor Reinhard Jahn. Afterwards, coverslips were washed 4× with ice-cold Tyrode, and were submerged in ice-cold 4% paraformaldehyde for 20 min. Fixation was finished at room temperature (20 min). Atto 647N was obtained as NHS-ester from Atto-Tec (Siegen). Goat anti-mouse or goat anti-rabbit Fab fragments (Jackson ImmunoResearch) were labeled with Atto by using a conventional NHS-labeling protocol (Invitrogen). The cultures were incubated with the Fab fragments in PBS containing 1.5% bovine serum albumin (PBS-BSA) in the dark, for 1 h, at room temperature. After exhaustive washing, we immunostained the preparations against native synaptic proteins to allow us to acutely identify the neuronal cells. For this purpose, we used the G96 polyclonal serum (anti-synaptophysin) when monoclonal antibodies were used for the STED experiments, and the 604.2 monoclonal antibody (anti-synaptotagmin) when polyclonals were used in STED; a Cy3-labeled secondary was used in both cases. All coverslips were finally mounted in Mowiol (6 g glycerol, 2.4 g Mowiol 4-88, 6 mL H₂O, 12 mL 0.2 M Tris pH 7.2 buffer). For surface staining, no detergents were used at any step of the immunostaining, to avoid the staining of intracellular structures; when intracellular structures were labeled, permeabilization was performed using 0.1% Triton-X-100. For live imaging experiments, 604.2 antibodies directed against synaptotagmin I were labeled with the dyes Oyster 550 (Synaptic Systems) or Atto 647N (dye obtained from Atto-Tec; the labeling was performed as above).

Microscopy

Neurons were imaged using a TCS STED fluorescence microscope from Leica Microsystems GmbH (Mannheim), using a 1.4 numerical aperture (NA), 100 \times objective (Leica). For STED imaging, excitation was performed with 635-nm diode laser, and depletion was achieved with a Spectra-Physics MaiTai tunable laser at 750 nm. Signal was detected using an avalanche photodiode. Confocal imaging of the Atto-labeled samples was performed using photomultipliers; their lower sensitivity results in less bright images (Figure 5) than for the photodiode. Confocal images were obtained with the same system as described earlier, except that excitation for the GFP chimeras and Cy3 was performed with 488-nm argon and 543-nm helium/neon laser lines, respectively. Oyster 550 was imaged using the same set-up as for Cy3. Confocal imaging of Atto 647N was performed under excitation using a 633-helium/neon laser line.

Two-color STED microscopy

We used a STED microscope equipped with a supercontinuum fiber laser source (SC-450 HP, Fianium), similar to a previously described set-up. Excitation laser beams (570 ± 5 nm for Atto 590 and 650 ± 5 nm for Atto 647N) and STED laser beams (720 ± 10 nm for Atto 590 and 755 ± 15 nm for Atto 647N) were all provided by the same laser source (36). Atto 590 was detected at 600–640 nm; Atto 647N was detected at 660–690 nm. A 1.4 NA, 100 \times objective lens was used (PL APO 100 \times /1.40–0.7 OIL, Leica Microsystems). We eliminated the crosstalk between the two detection channels by linear unmixing. The images shown are otherwise raw data (no filtering was applied).

Thin-section embedding and processing

The melamin-embedding technique was performed as described (21). Neuronal cultures were labeled as described in *Results*, and were then chemically fixed (2.5% glutaraldehyde and 4% paraformaldehyde in PBS). They were afterwards submerged in a solution containing 68% 2,4,6-tris[bis(methoxymethyl)amino]-1,3,5-triazine (melamin; TCI Europe nv) and 2.4% *p*-toluenesulfonic acid (Sigma-Aldrich), in water. The mixture was allowed to harden for 24 h at 22 $^{\circ}$ C, followed by 24 h at 40 $^{\circ}$ C and 48 h at 60 $^{\circ}$ C. The coverslips were then removed, and the blocks were processed in ultrathin (80–90 nm) sections by using a conventional ultramicrotome (EM UC6) and diamond knife (Ultra 35 $^{\circ}$, DiS-Galetzka). The sections were collected on gelatin-coated coverslips, and imaged (set-up described above) after embedding in Mowiol. For electron microscopy, cell cultures were grown on Thermanox coverslips (Plano), stimulated in the presence of 10 μ M FM 1-43 (Biotium), allowed to recover for 30 seconds, and fixed, photoconverted and processed for electron microscopy as described (37).

Data analysis

Data analysis was performed by custom-written procedures, in Matlab (The Mathworks Inc.). For the identification of protein cluster size (Figure 1), the line scans were manually drawn on all fluorescent spots, which appeared brighter than the background. Lorentzian curves were fit on the line scan profiles (10), and the FWHM was obtained from the fits. Only spots that were well-fit by the Lorentzian function (the absolute difference between the data and the fit is less than 2% of the integral of the fit) were accepted for the FWHM measurement. For the autocorrelation analysis, a rectangular region of interest containing the immunostained axon was manually selected. A copy of the region of interest was superimposed on it, as described in the main text, and automatically shifted, pixel-by-pixel; the Pearson's correlation coefficient was calculated at every shift. Histograms of pixel intensity in the axons were generated in Matlab as follows. Rectangular regions of interest were selected, containing the axons to be analyzed. The axonal area was automatically determined from the confocal image of the Atto dye, by use of an adaptive threshold above the mean image background value; background was calculated from rectangular regions of interest selected by the user in image areas where no fluorescence could be visually detected. All other data analysis routines were performed by custom-written procedures, as detailed in *Results*. All values are given in mean \pm standard error of the mean (SEM). Graphs,

curve fits and statistical analysis were carried out with GraphPad Prism 5.0 (GraphPad Software).

Acknowledgments

We thank R. Jahn for the kind gift of antisynaptic vesicle protein antibodies. We thank C. Schäfer for technical assistance and S. Saka for help with experiments. S. O. R. thanks A. Bock for excellent assistance. The work was supported by the European Research Council under the European Community's Seventh Framework Programme (FP7/2007-2013)/ERC grant agreement No. 201936, and by a Research grant from the Deutsche Forschungsgemeinschaft (RI 1967/1-1, Super-resolution investigation of synaptic vesicle recycling).

Supporting Information

Additional Supporting Information may be found in the online version of this article:

Figure S1: Background spot detection in live imaging. Preparations were labeled as in Figure 2, and live movies were generated (imaging at a frequency of 0.5 Hz, for 2 min). A small area was cropped, and a movie was generated in which the scaling was adjusted from 5 to 15 arbitrary units (values below 5 appearing as black, and values above 15 as white). The movie is included as Movie S1. A) A single frame of the movie. The red arrowheads point to five background spots, which persist throughout the movie. The green arrowhead points to a spot, which disappeared after \sim 5 seconds (20 frames). B) Sum of the first 8 frames of the movie. C) Sum of frames 21–28. Note the disappearance of the spot indicated by the green arrowhead. Size bar = 1 μ m. D) We have analyzed the fluorescence of the five spots indicated by the red arrowheads (by calculating the average fluorescence in circular ROIs of 20-pixel radius superimposed on the spots; indicated in red). We compared the fluorescence of the spots with that of six random empty areas (black). The disappearing spot (corresponding to an antibody that washes away or bleaches) reaches the ground levels after the first few frames (green). E) Averages (\pm SEM) for the persistent spots and the empty background. Clearly, the change in signal even for a relatively dim spot is measurable (green).

Figure S2: Example for the filtering procedure, as described in the main text. The original image areas (left panels) are filtered by using an *unsharp* filter (Matlab), to remove background. The filter subtracts a blurred version of the image from the original image, therefore rendering a sharper, largely background-corrected, version of the original image. The images were then smoothed by use of an averaging filter, and an automatic threshold (set to a value 1.5-fold higher than the mean intensity of the region under investigation) was used to identify the fluorescent spots in both channels. The spots above threshold are shown in the middle panels (filtered image), and the total area above threshold is shown in white in the panels on the right. Note that the filtering procedure faithfully recovers the intense spots that are visually identifiable. Size bar = 500 nm.

Figure S3: Comparison of the intensity of single antibodies (black) and vesicles (red). Data plotted from Willig et al. (10). The vesicle intensity distribution was deconvolved using the single antibody distribution, thereby obtaining a vesicle intensity distribution expressed in number of antibodies per vesicle (blue). The deconvolution analysis was performed using Monte Carlo simulations, as follows: the intensities of 100 vesicles and 100 single antibodies were generated from the two intensity distributions. For each of the vesicles, we combined single antibodies until their summed intensity equaled that of the vesicle; the calculation was repeated 10^3 times for each vesicle, and a mean number of antibodies per vesicle was obtained (for the particular vesicle). The calculation was then performed for all vesicles, and a distribution of vesicle intensities expressed in number of antibodies was thus obtained. The whole process was then repeated 10^4 times; the graph (blue) represents the average of the 10^4 distributions. The mean number of antibodies per vesicle is 5.9 ± 0.47 (mean \pm SEM).

Figure S4: Example of maximal correlation in two-color STED. The surface pool of synaptotagmin was labeled by Atto 647N-coupled

antibodies, and the cells were fixed and immunostained using Atto 590-coupled secondary antibodies (anti-mouse). An example image is shown. Scale bar = 1 μm . The correlation coefficient for the two stainings is ~ 0.32 . Graph represents the mean \pm SEM from 44 axonal areas, from five independent experiments.

Figure S5: Surface spot density versus overexpression. Analysis of identifiable STED spots (clusters) present in different axonal areas in preparations expressing synaptophysin, synaptophysin-pHluorin or synaptotagmin-citrine. The density of spots (determined as in Figure S2) is plotted against the average axonal intensity in the particular axon region. Each spot corresponds to one axonal region [region of interest (ROI)], typically of at least 2 μm^2 .

Movie S1: Preparations were labeled as in Figure 2, and live movies were generated (imaging at a 0.5 Hz frequency, for 2 min). A small area was cropped, and a movie was generated in which the scaling was adjusted from 5 to 15 arbitrary units (values below 5 appearing as black, and values above 15 as white). Note that the spatial drift in the movie is not corrected for in the movie; the drift was corrected in all analysis performed (Figure S1).

Please note: Wiley-Blackwell are not responsible for the content or functionality of any supporting materials supplied by the authors. Any queries (other than missing material) should be directed to the corresponding author for the article.

References

- Rizzoli SO, Betz WJ. Synaptic vesicle pools. *Nat Rev Neurosci* 2005;6:57–69.
- Sudhof TC. The synaptic vesicle cycle. *Annu Rev Neurosci* 2004;27:509–547.
- Miesenböck G, De Angelis DA, Rothman JE. Visualizing secretion and synaptic transmission with pH-sensitive green fluorescent proteins. *Nature* 1998;394:192–195.
- Ryan TA. Presynaptic imaging techniques. *Curr Opin Neurobiol* 2001;11:544–549.
- Li Z, Murthy VN. Visualizing postendocytic traffic of synaptic vesicles at hippocampal synapses. *Neuron* 2001;31:593–605.
- Sankaranarayanan S, Ryan TA. Real-time measurements of vesicle-SNARE recycling in synapses of the central nervous system. *Nat Cell Biol* 2000;2:197–204.
- Wienisch M, Klingauf J. Vesicular proteins exocytosed and subsequently retrieved by compensatory endocytosis are nonidentical. *Nat Neurosci* 2006;9:1019–1027.
- Granseth B, Odermatt B, Royle SJ, Lagnado L. Clathrin-mediated endocytosis is the dominant mechanism of vesicle retrieval at hippocampal synapses. *Neuron* 2006;51:773–786.
- Fernández-Alfonso T, Kwan R, Ryan TA. Synaptic vesicles interchange their membrane proteins with a large surface reservoir during recycling. *Neuron* 2006;51:179–186.
- Willig KI, Rizzoli SO, Westphal V, Jahn R, Hell SW. STED microscopy reveals that synaptotagmin remains clustered after synaptic vesicle exocytosis. *Nature* 2006;440:935–939.
- Donnert G, Keller J, Medda R, Andrei MA, Rizzoli SO, Lüthmann R, Jahn R, Eggeling C, Hell SW. Macromolecular-scale resolution in biological fluorescence microscopy. *Proc Natl Acad Sci U S A* 2006;103:11440–11445.
- Kraszewski K, Mundigl O, Daniell L, Verderio C, Matteoli M, De Camilli P. Synaptic vesicle dynamics in living cultured hippocampal neurons visualized with CY3-conjugated antibodies directed against the luminal domain of synaptotagmin. *J Neurosci* 1995;15:4328–4342.
- Kraszewski K, Daniell L, Mundigl O, De Camilli P. Mobility of synaptic vesicles in nerve endings monitored by recovery from photobleaching of synaptic vesicle-associated fluorescence. *J Neurosci* 1996;16:5905–5913.
- Fernández-Alfonso T, Ryan TA. The kinetics of synaptic vesicle pool depletion at CNS synaptic terminals. *Neuron* 2004;41:943–953.
- Balaji J, Ryan TA. Single-vesicle imaging reveals that synaptic vesicle exocytosis and endocytosis are coupled by a single stochastic mode. *Proc Natl Acad Sci U S A* 2007;104:20576–20581.
- Harata N, Pyle JL, Aravanis AM, Mozhayeva M, Kavalali ET, Tsien RW. Limited numbers of recycling vesicles in small CNS nerve terminals: implications for neural signaling and vesicular cycling. *Trends Neurosci* 2001;24:637–643.
- Fernández-Alfonso T, Ryan TA. A heterogeneous “resting” pool of synaptic vesicles that is dynamically interchanged across boutons in mammalian CNS synapses. *Brain Cell Biol* 2008;36:87–100.
- Schikorski T, Stevens CF. Morphological correlates of functionally defined synaptic vesicle populations. *Nat Neurosci* 2001;4:391–395.
- Westphal V, Rizzoli SO, Lauterbach MA, Kamin D, Jahn R, Hell SW. Video-rate far-field optical nanoscopy dissects synaptic vesicle movement. *Science* 2008;320:246–249.
- Miller TM, Heuser JE. Endocytosis of synaptic vesicle membrane at the frog neuromuscular junction. *J Cell Biol* 1984;98:685–698.
- Punge A, Rizzoli SO, Jahn R, Wildanger J, Meyer L, Schönle A, Kastrop L, Hell S. 3D reconstruction of high-resolution STED microscope images. *Microsc Res Tech* 2008;71:644–650.
- Donnert G, Keller J, Wurm CA, Rizzoli SO, Westphal V, Schönle A, Jahn R, Jakobs S, Eggeling C, Hell SW. Two-color far-field fluorescence nanoscopy. *Biophys J* 2007;92:L67–L69.
- Bethani I, Lang T, Geumann U, Sieber JJ, Jahn R, Rizzoli SO. The specificity of SNARE pairing in biological membranes is mediated by both proof-reading and spatial segregation. *EMBO J* 2007;26:3981–3992.
- Mani M, Ryan TA. Live imaging of synaptic vesicle release and retrieval in dopaminergic neurons. *Front Neural Circuits* 2009;3:3.
- Fredj NB, Burrone J. A resting pool of vesicles is responsible for spontaneous vesicle fusion at the synapse. *Nat Neurosci* 2009;12:751–758.
- Bennett MK, Calakos N, Kreiner T, Scheller RH. Synaptic vesicle membrane proteins interact to form a multimeric complex. *J Cell Biol* 1992;116:761–775.
- Takamori S, Holt M, Stenius K, Lemke EA, Grønborg M, Riedel D, Urlaub H, Schenck S, Brügger B, Ringler P, Müller SA, Rammner B, Gräter F, Hub JS, De Groot BL et al. Molecular anatomy of a trafficking organelle. *Cell* 2006;127:831–846.
- Gandhi SP, Stevens CF. Three modes of synaptic vesicular recycling revealed by single-vesicle imaging. *Nature* 2003;423:607–613.
- Zhu Y, Xu J, Heinemann SF. Two pathways of synaptic vesicle retrieval revealed by single-vesicle imaging. *Neuron* 2009;61:397–411.
- Aravanis AM, Pyle JL, Tsien RW. Single synaptic vesicles fusing transiently and successively without loss of identity. *Nature* 2003;423:643–647.
- Harata NC, Aravanis AM, Tsien RW. Kiss-and-run and full-collapse fusion as modes of exo-endocytosis in neurosecretion. *J Neurochem* 2006;97:1546–1570.
- Klingauf J, Kavalali ET, Tsien RW. Kinetics and regulation of fast endocytosis at hippocampal synapses. *Nature* 1998;394:581–585.
- Pyle JL, Kavalali ET, Piedras-Rentería ES, Tsien RW. Rapid reuse of readily releasable pool vesicles at hippocampal synapses. *Neuron* 2000;28:221–231.
- Zhang Q, Li Y, Tsien RW. The dynamic control of kiss-and-run and vesicular reuse probed with single nanoparticles. *Science* 2009;323:1448–1453.
- Richards DA, Guatimosim C, Rizzoli SO, Betz WJ. Synaptic vesicle pools at the frog neuromuscular junction. *Neuron* 2003;39:529–541.
- Wildanger D, Rittweger E, Kastrop L, Hell SW. STED microscopy with a supercontinuum laser source. *Optics Express* 2008;16:9614–9621.
- Rizzoli SO, Betz WJ. The structural organization of the readily releasable pool of synaptic vesicles. *Science* 2004;303:2037–2039.